Stress relaxation in thin films due to grain boundary diffusion and dislocation glide

Ayas, Can

Chapter 2

Methodology

Dislocation dynamics (DD) method is briefly outlined in this chapter. DD is a computational framework to study plastic flow in materials by collective motion of dislocations. Dislocations are treated individually as displacement discontinuities in an otherwise perfect elastic continuum that gives rise to characteristic displacement and stress fields. Dislocations are utilized in order to model slip and 'misfit' due to presence of extra material. The effects of boundaries on elastic field quantities are taken into account with the use of superposition principle [2]. The motion of dislocations manifests the permanent inelastic deformation which is driven by forces due to interaction with other dislocations and external loads. Dislocation motion, generation and annihilation are characterized by constitutive rules which represent fundamental atomistic features of the dislocations.

2.1 Introduction

DD is a meso-scale computational tool which is developed for plasticity problems where time and length scales involved renders atomistic approaches such as molecular dynamics impractical due to the enormous number of atoms involved. In contrast, conventional continuum approaches are inappropriate since the deformation is highly inhomogeneous due to distinct patterning of dislocation ensemble. DD bridges the continuum and atomistic scales in order to accurately describe the inelastic deformation phenomena and hence becomes an efficient computational tool in the length scale range roughly from fractions of to few micrometers. In DD framework the material is considered as an elastic continuum which contains dislocations as discrete entities. The way the dislocation structure develops takes into account the fundamental atomistic features of dislocations as line defects in a perfect crystal through a set of constitutive rules.

2.2 Dislocation representation

In real materials dislocation can be conceptualized as a line tracing the atoms that exhibit a lattice mismatch with the host crystal. The lattice mismatch creates unique distortion quantified by the Burgers vector, $\boldsymbol{b}$ which has a magnitude equal to the interatomic spacing. Since $\boldsymbol{b}$ should be conserved, dislocations cannot terminate within the crystal but form either closed loops or cease at the free surface by creating a surface step. In a continuum framework the notion of Burgers vector is introduced with a displacement discontinuity and stated as

$$b_i = \oint \frac{\partial u_i}{\partial c} dc, \tag{2.1}$$

where u_i is the displacement vector field and the integral is taken around a contour that encloses the dislocation line. The plane on which the dislocation resides is identified with its unit normal vector m_i. Throughout the coming chapters two classes of dislocation loops with different geometrical properties will be the focus of attention. The first class of dislocations are the glide loops which are typically emitted from Frank-Read sources and their motion manifests the slip across glide planes which is illustrated in figure 2.1(a) while 'misfit' loops can be regarded as a result of dislocation climb motion that embody the presence of extra material along the dislocation plane which is illustared in figure 2.1(b).

For two dimensional (2D) plane strain problems which the current study is limited to, the projection of three dimensional loop onto the plane of paper is considered. Hence in 2D the dislocation loop is represented by a dipole of two edge dislocations. For a glide dipole, b_i is orthogonal to the glide plane normal m_i. The 'misfit' dipole also

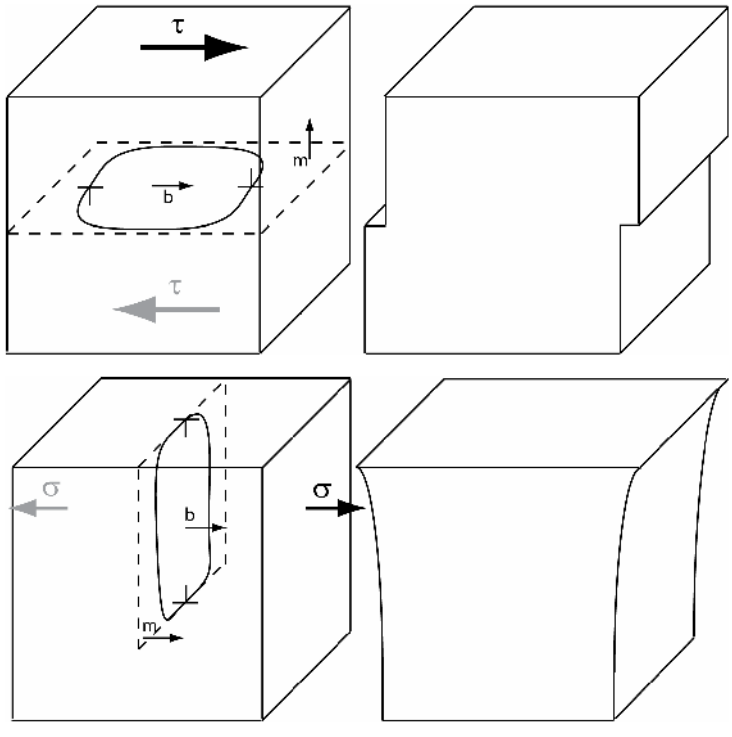

Figure 2.1: Schematic representation of glide (a). Dislocation loop is shown on the left column which expands under the effect of resolved shear stress τ. On the right column surface steps have been formed when dislocation loop reaches the material boundaries. Schematic representation of 'misfit' (b). Dislocation loop is given in left column expands under the resolved normal stress σ. The deformation of material due to presence of dislocation is illustrated on the right column.

consists of a pair of edge dislocations, however b_i is now parallel to m_i. Accordingly both dipoles create a displacement field that is discontinuous along the slip/'misfit' plane. The displacement discontinuity is tangential to m_i for the glide dipole whereas it is normal to m_i in the 'misfit' dipole. The displacement field of a glide dislocation in infinite space is well known e.g. [1] and given by

$$u_1(x_1, x_2) = \frac{b}{2\pi(1-\nu)}\left(\frac{1}{2}\frac{x_1 x_2}{{x_1}^2 + {x_2}^2} - (1-\nu)\tan^{-1}(\frac{x_1}{x_2})\right) \tag{2.2}$$

$$u_2(x_1, x_2) = \frac{b}{2\pi(1-\nu)}\left(\frac{1}{2}\frac{{x_2}^2}{{x_1}^2 + {x_2}^2} - \frac{1}{4}(1-2\nu)\ln(\frac{{x_1}^2 + {x_2}^2}{b})\right) \tag{2.3}$$

for a dislocation positioned at the origin of a Cartesian coordinate system where b is the magnitude of the Burgers vector and ν is the Poisson's ratio. On the contrary the x_1 component of displacement field of a 'misfit' edge dislocation differs subtly by the

orientation of multivalued portion of arc tangent function and given as,

$$u_1 = \frac{b}{2\pi(1-\nu)}\left(\frac{1}{2}\frac{x_1 x_2}{x_1^2 + x_2^2} + (1-\nu)\tan^{-1}(\frac{x_2}{x_1})\right). \tag{2.4}$$

In figure 2.2 these displacement fields for the two different types of dipoles are illustrated.

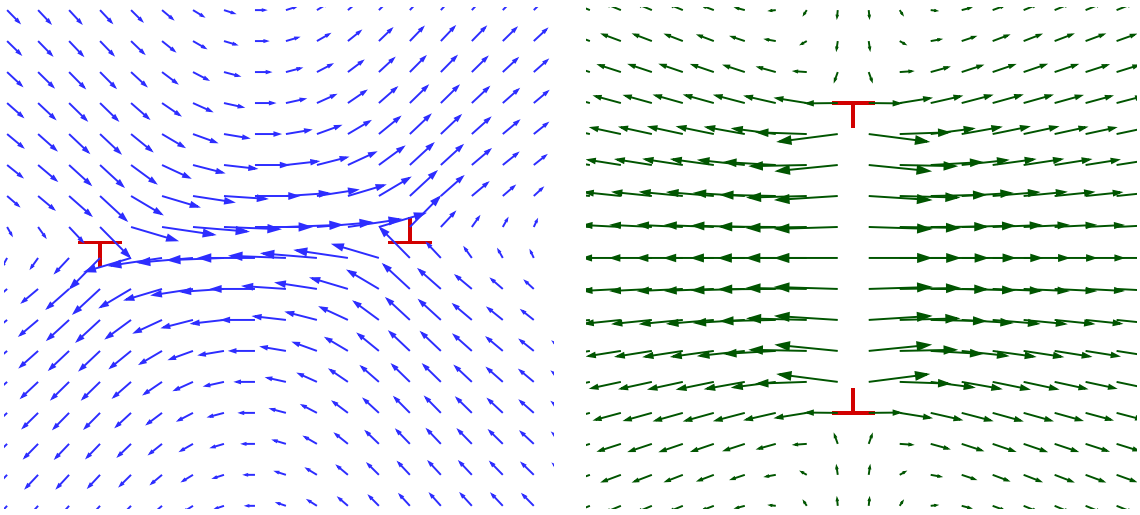

(a) (b)

Figure 2.2: Displacement vector plots in infinite space for the glide dipole where the displacements are calculated according to equations (2.2) and (2.3) (a), for the 'misfit' dipole according to equations (2.4) and (2.3) (b).

2.3 Stress Fields for Edge Dislocations

The stress fields around an edge dislocation in an infinite space can be obtained by first calculating the strain fields,

$$2\varepsilon_{ij} = u_{i,j} \tag{2.5}$$

and then using the linear elastic constitutive law for the isotropic case,

$$\sigma_{ij} = \frac{E}{1+\nu}\left[\varepsilon_{ij} + \frac{\nu}{1-2\nu}\varepsilon_{kk}\delta_{ij}\right] \tag{2.6}$$

where E is the elastic modulus, ν is Poisson's ratio and δ_{ij} is the Kronecker delta. For both classes of edge dislocations the strain fields and therefore the stress fields are iden-

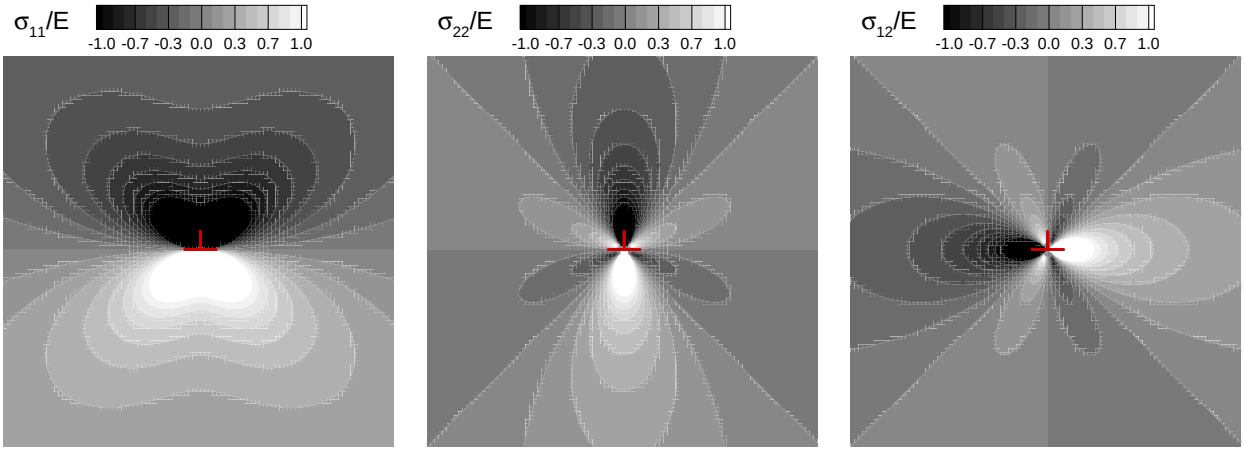

(a) (b) (c)

Figure 2.3: Contour plots for the σ_{11} (a) σ_{22} (b) and σ_{12} (c) components of the stress tensor for an edge dislocation at origin.

tical and read as

$$\sigma_{11} = -\frac{Eb}{4\pi(1-\nu^2)}\frac{x_2(3{x_1}^2+{x_2}^2)}{({x_1}^2+{x_2}^2)^2} \tag{2.7}$$

$$\sigma_{22} = \frac{Eb}{4\pi(1-\nu^2)}\frac{x_2({x_1}^2-{x_2}^2)}{({x_1}^2+{x_2}^2)^2} \tag{2.8}$$

$$\sigma_{12} = \frac{Eb}{4\pi(1-\nu^2)}\frac{x_1({x_1}^2-{x_2}^2)}{({x_1}^2+{x_2}^2)^2} \tag{2.9}$$

which are visualized by contour plots in figure 2.3. All components of the stress tensor are singular at the dislocation position. Obviously this singularity is not physical but arises due to linear elastic continuum analysis over the crystal distortions that are incompatible. Moreover elastic field quantities in the vicinity of dislocation should be handled with care since the atomistic nature of a dislocation reminds us neither the smalls strain assumption nor omitting the quadratic terms in equation (2.5) is validated. However the atomistic studies revealed that a cylindrical core volume around the dislocation loop with non–linear and finite strains has a radius around $r_c \approx 2b$. Thus a few nanometers away from the dislocations, continuum linear elasticity is highly accurate and hence the atomistic configuration of the material no longer needs to be resolved.

2.4 Superposition Principle

Although stress and displacement fields for dislocations in infinite space are given by closed–form solutions specified above, analytical solution for a solid enclosed by an

arbitrary surface is not available. However superposition principle formulated by Van der Giessen and Needleman [2] is a general approach for the solution of dislocation field quantities in boundary value problems.

For an elastic solid V with a surface ∂V illustrated in figure 2.4(a), the boundary conditions for the general case are prescribed tractions, T_i^0 on some portion of the boundary ∂V^T and prescribed displacements, U_i^0 on the remaining of the surface ∂V^U, i.e. $\partial V = \partial V^T \cup \partial V^U$. The elastic fields for the problem at hand can be decomposed into fields for the dislocation ensemble in infinite space denoted by $\tilde{(\,)}$ (see figure 2.4(b)) and elastic fields due boundary corrections denoted by $\hat{(\,)}$ (see figure 2.4(c)). For instance for the case of stress, decomposition reads

$$\sigma_{ij} = \tilde{\sigma}_{ij} + \hat{\sigma}_{ij}. \tag{2.10}$$

In order to identify $\hat{\sigma}_{ij}$, the following boundary value problem should be considered. The traction on the surface ∂V^T caused by the ensemble of dislocations in infinite space can be found as

$$\tilde{t}_i = \sum_{I=1}^{N} \tilde{\sigma}_{ij}^{(I)} n_j \tag{2.11}$$

where I is the dislocation index that runs from 1 to number of dislocations N and n_i is the unit surface normal. Since the tractions are prescribed to T_i^0 the complimentary tractions for the problem shown in figure 2.4(c) should be

$$\hat{t}_i = T_i^0 - \tilde{t}_i \tag{2.12}$$

on ∂V^T. Similarly the prescribed displacements on ∂V^U become

$$\hat{u}_i = U_i^0 - \tilde{u}_i. \tag{2.13}$$

Thus the solution of the boundary correction becomes a standard boundary value problem itself which is governed by the principle of virtual work

$$\int_{\partial V} \hat{t}_i \delta \hat{u}_i dA = \int_V \hat{\sigma}_{ij} \delta \hat{\varepsilon}_{ij} dV, \tag{2.14}$$

together with the boundary conditions equations (2.12) and (2.13). The discretization of integrals in equation (2.14) naturally leads to the numerical solution by the finite element method.

2.5 Dislocation Motion & Constitutive Rules

Dislocation motion is driven by the thermodynamic force on a dislocation – the so called Peach-Koehler force – which is due to externally applied loading and the stress fields

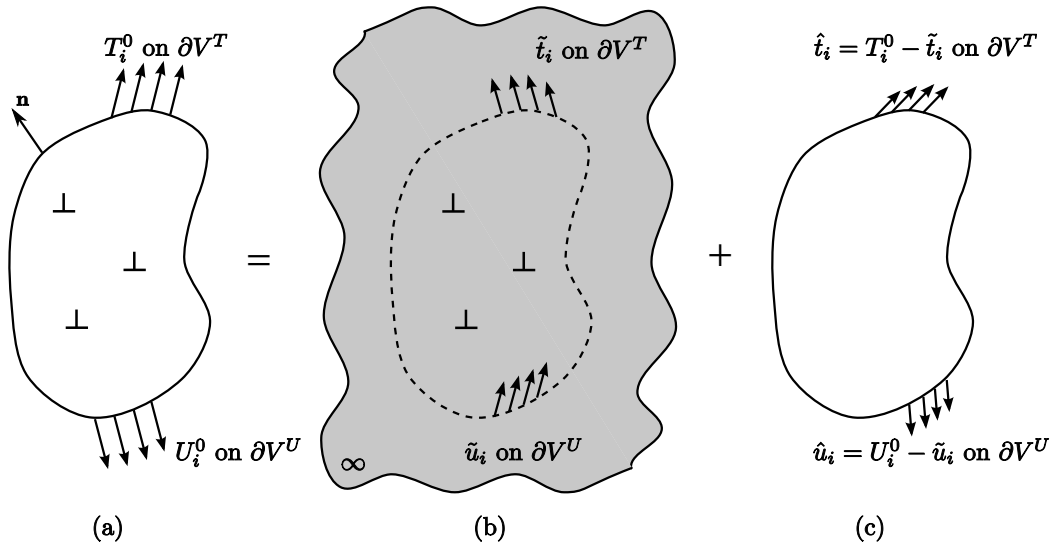

Figure 2.4: The schematic illustration of superposition principle where for elastic fields of the solid with dislocations (a) can be decomposed to problem of infinite solid and the complimentary problem with a solid with no dislocations.

of other dislocations. In the framework of superposition principle Van der Giessen and Needleman [2] derived the Peach–Koehler force by considering the variations in potential energy due to variations in dislocation positions. The component of this force in the plane of dislocation is

$$f^{(I)} = m_i^{(I)} \left(\hat{\sigma}_{ij} + \sum_{J \neq I} \tilde{\sigma}_{ij}^{(I)} \right) b_j^{(I)} \tag{2.15}$$

where the index I runs over the total number of dislocations in the system. It is important to note that although the stress field of a dislocation is singular the Peach–Koehler force is not because it does not depend on the stress field of itself. Equation (2.15) can be rewritten in a more compact form

$$f^{(I)} = \tau^{(I)} b^{(I)} \tag{2.16}$$

by defining $\tau^{(I)}$, the resolved shear stress on the particular slip plane of interest as

$$\tau^{(I)} = m_i^{(I)} \left(\hat{\sigma}_{ij} + \sum_{J \neq I} \tilde{\sigma}_{ij}^{(I)} \right) n_j^{(I)} \tag{2.17}$$

where $n_i^{(I)}$ is the unit vector in the direction of $b_i^{(I)}$. The current study assumes quasi–static deformation in the solid. Moreover inertial effects becomes important at a time scale much smaller than the one associated with the dislocation motion. Therefore inertial effects of dislocation motion is omitted. In the absence of inertia, phonons are

assumed to create a drag force counteracting on the Peach-Koehler force as

$$f^{(I)} - Bv^{(I)} = \rho\dot{v}^{(I)} = 0 \tag{2.18}$$

and therefore the dislocation glide velocity $v^{(I)}$ is given as

$$v^{(I)} = f^{(I)}/B \tag{2.19}$$

where B is the drag coefficient. Metals usually posses some density of dislocations even at the undeformed state. Upon the application of loads new dislocations are generated and dislocation density increases. In the present DD framework nucleation occurs from point sources which represents a Frank–Read segment pinned at two points. The nucleation occurs by bowing out of the segment which in 2D corresponds to emission of a dipole a when the resolved shear stress, τ exceeds the source strength, τ_{nuc} for a duration of nucleation time t_{nuc}. The schematic of the nucleation event is given in figure 2.5. The dipole is initially separated by a distance

$$L_{\text{nuc}} = \frac{E}{4\pi(1-\nu^2)}\frac{b}{\tau} \tag{2.20}$$

so that there the attractive forces between the two ends of the dipole are equilibrated by the applied shear stress, τ. Dislocations with opposite signs are annihilated when they are closer than $6b$ to each other granted they live on the identical slip plane. In contrast dislocations from different slip planes pin each other which gives way to hardening of material as the dislocation density increases.

For a 'misfit' edge dislocation the critical component of Peach–Koehler force still governed by equation (2.15) however due to the different orientation of 'misfit' plane it is convenient to rewrite equation (2.15) similar to equation (2.16) as

$$f^{(I)} = \sigma^{(I)}b^{(I)} \tag{2.21}$$

where σ is now defined as the stress component normal to the $m_i^{(I)}$ i.e.

$$\sigma^{(I)} = m_i^{(I)}\left(\hat{\sigma}_{ij} + \sum_{J\neq I}\tilde{\sigma}_{ij}^{(I)}\right)n_j^{(I)} \tag{2.22}$$

that is responsible from 'climb' of 'misfit' dislocations (see figure 2.1). The 'climb' motion of 'misfit' dislocation is explored in Chapter 4.

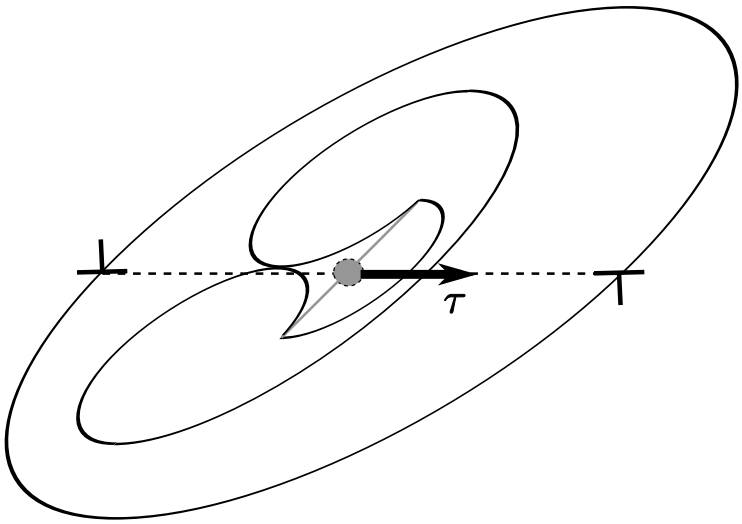

Figure 2.5: Schematic illustration of a Frank–Read source which is a dislocation segment is pinned between two points. Nucleation happens when the segment becomes unstable due to resolved shear stress and bow around itself. Partial annihilation leaves a loop and a copy of the original segment.

Bibliography

[1] J.P. Hirth and J. Lothe. *Theory of Dislocations*. New York: McGraw-Hill, 1968.

[2] E. Van der Giessen and A. Needleman. Discrete dislocation plasticity: a simple planar model. *Modelling and Simulation in Materials Science and Engineering*, 3(5):689–735, 1995.